

Diurnal variation of midlatitudinal NO₃ column abundance over table mountain facility, California

C. M. Chen^{1,*}, R. P. Cageao^{1,**}, L. Lawrence^{2,***}, J. Stutz², R. J. Salawitch^{1,****}, L. Jourdain^{1,*****}, Q. Li^{1,2}, and S. P. Sander¹

¹Jet Propulsion Laboratory, California Institute of Technology, Pasadena, California, USA

²University of California, Los Angeles, California, USA

* now at: Potsdam Institute for Climate Impact Research, Potsdam, Germany

** now at: NASA Langley Research Center, Hampton, Virginia, USA

*** now at: California Air Resources Board, Sacramento, California, USA

**** now at: University of Maryland, College Park, Maryland, USA

***** now at: Laboratoire de Physique et Chimie de l'Environnement et de l'Espace, Université d'Orléans/CNRS, France

Received: 22 June 2010 – Published in Atmos. Chem. Phys. Discuss.: 26 August 2010

Revised: 19 January 2011 – Accepted: 27 January 2011 – Published: 2 February 2011

Abstract. The column abundance of NO₃ was measured over Table Mountain Facility, CA (34.4° N, 117.7° W) from May 2003 through September 2004, using lunar occultation near full moon with a grating spectrometer. The NO₃ column retrieval was performed with the differential optical absorption spectroscopy (DOAS) technique using both the 623 and 662 nm NO₃ absorption bands. Other spectral features such as Fraunhofer lines and absorption from water vapor and oxygen were removed using solar spectra obtained at different airmass factors. We observed a seasonal variation, with nocturnally averaged NO₃ columns between $5 - 7 \times 10^{13}$ molec cm⁻² during October through March, and $5 - 22 \times 10^{13}$ molec cm⁻² during April through September. A subset of the data, with diurnal variability vastly different from the temporal profile obtained from one-dimensional stratospheric model calculations, clearly has boundary layer contributions; this was confirmed by simultaneous long-path DOAS measurements. However, even the NO₃ columns that did follow the modeled time evolution were often much larger than modeled stratospheric partial columns constrained by realistic temperatures and ozone concentrations. This discrepancy is attributed to substantial tropospheric NO₃ in the free troposphere, which may have the same time dependence as stratospheric NO₃.

1 Introduction

NO₃ plays a significant role in the nocturnal chemistry of the stratosphere and troposphere. In the stratosphere, it influences the partitioning of active nitrogen species NO and NO₂ (NO_x), where NO_x is an important component in catalytic ozone loss cycles. The primary source of NO₃ is a reaction between NO₂ and O₃ (Reaction R1), and it is consumed by an additional reaction with NO₂ to form the reservoir species N₂O₅ (Reaction R2).



So as shown in Reaction (R2), NO₂, NO₃, and N₂O₅ are in equilibrium. The subsequent removal of N₂O₅ via a heterogeneous reaction with water on the surfaces of ice particles to form nitric acid, also a reservoir species for NO_x but with longer lifetime, contributes to NO_x removal. The thermal decomposition of N₂O₅ is an additional significant source of NO₃ in the upper stratosphere. Since NO₃ photodissociates extremely rapidly at wavelengths less than about 640 nm, we observe significant concentrations only at night.

In the troposphere the same formation and destruction reactions occur with heterogeneous loss of N₂O₅ occurring on any moist aerosol surface. There is also negligible NO₃ during sunlit hours except for extremely polluted urban settings (Geyer et al., 2003). In the boundary layer, NO₃ additionally is an important nighttime oxidant because it reacts rapidly with many biogenic hydrocarbons such as alkenes, aldehydes and terpenes (Atkinson, 1991; Wayne et al., 1991).



Correspondence to: C. M. Chen
(claudine.chen+acp@googlemail.com)

Interest in the role played by NO₃ in atmospheric chemistry increased significantly following the first reports of its detection in the stratosphere and troposphere by Noxon et al. (1978, 1980) and Platt et al. (1980). Since then, other measurements of atmospheric NO₃ column at low and mid-latitudes at urban-influenced and remote ground-based sites have been made by using the Moon as a light source and employing differential optical absorption spectroscopy (DOAS) (Aliwell and Jones, 1996a,b, 1998; Lal et al., 1993; Renard et al., 2001; Solomon et al., 1989). Also, vertical concentration profiles of NO₃ have been inferred from ground-based measurements by observing NO₃ in the slant column during sunrise with direct lunar, zenith sky, and off-axis methods (Allan et al., 2002; Coe et al., 2002; Smith and Solomon, 1990; Smith et al., 1993; von Friedeburg et al., 2002; Weaver et al., 1996). As the solar terminator sweeps from the upper atmosphere down to the surface, photolysis progressively decreases the column of NO₃, leaving only the column that lies below the terminator altitude. Additionally, stratospheric profiles of NO₃ have been obtained from the SAGE III (Stratospheric Aerosol and Gas Experiment) and SCIAMACHY (SCanning Imaging Absorption spectrometer for Atmospheric Cartography) Amekudzi et al., 2005) satellite instruments using lunar occultation, and the GOMOS (Global Ozone Monitoring by Occultation of Stars) (Hauchecorne et al., 2005; Marchand et al., 2004) satellite instrument using stellar occultation.

A number of measurements have confirmed the role of NO₃–N₂O₅ chemistry in the nocturnal boundary layer (Aldener et al., 2006; Allan et al., 2000; Ambrose et al., 2007; Ayers and Simpson, 2006; Brown et al., 2003, 2004; Carslaw et al., 1997a; Geyer et al., 2001; Geyer and Platt, 2002; Li et al., 2008; Matsumoto et al., 2006; Mihelcic et al., 1993; Nakayama et al., 2008; Penkett et al., 2007; Platt et al., 1981; Smith et al., 1995; Stutz et al., 2004; Vrekoussis et al., 2007; Wang et al., 2006). Fewer have probed above the boundary layer, essentially those using LP-DOAS (Carslaw et al., 1997b), aircraft measurements (Brown et al., 2007a,b) and zenith sky measurements at sunrise (Allan et al., 2002; Coe et al., 2002; von Friedeburg et al., 2002). Due to this relative lack of measurements above the boundary layer, the role of NO₃–N₂O₅ chemistry in the free and upper troposphere has not been quantitatively tested.

Our focus is on the quantification of NO₃ in the free troposphere. We deduce time-resolved estimates of free tropospheric NO₃ using measurements of total column NO₃, observations of the boundary layer concentration of NO₃, with stratospheric columns provided by a model. Specifically, we present results of simultaneous measurements of NO₃ column by lunar occultation with the DOAS technique, and surface concentration of NO₃ using LP-DOAS, taken on evenings near full moon in August and September 2004 over Table Mountain Facility (TMF), California. Using a climatology for ozone concentration and temperature constructed from over 10 years of lidar measurements at our measure-

ment site, we get stratospheric partial columns from a stratospheric model shown to be consistent with SAGE III satellite lunar occultation measurements of NO₃. We also used global chemistry and transport model GEOS-Chem to characterize the time evolution and vertical distribution of NO₃ in the troposphere for various locations. The full dataset of NO₃ column measurements was taken from May 2003 through September 2004, and we characterized the magnitude and variability of column NO₃ at TMF.

2 Experiment description

2.1 Location and measurement frequency

We have acquired direct lunar occultation measurements of the NO₃ column at Table Mountain Facility (TMF), California (34.4° N, 117.7° W) at an altitude of 2280 m. TMF is in the San Gabriel Mountains north of the Los Angeles Basin and south of the Mojave Desert; therefore it is influenced by clean and polluted air masses. Optimal measurements were acquired within the 5 day period centered on full moon. Full moon conditions offer the longest period of moonlit evening hours and the highest signal to noise due to the intensity of reflected sunlight with lunar phase angle opposition effect (Hapke et al., 1993). Observations from May 2003 through September 2004 consisted of three evenings for each full moon event, weather permitting. Measurements during 16 out of 18 full moon events were made, resulting in 40 days of data, out of a possible 90 days.

2.2 Lunar occultation measurement

2.2.1 Instrument configuration

The experimental apparatus (Cageao et al., 2001) is shown in Fig. 1. Light was collected by a heliostat and directed into an off-axis telescope with 3 × magnification. The 7-cm diameter collimated beam from the telescope was transmitted through a condensing lens, a shutter and order sorting filter (Schott GG-400 glass) to a 0.3 m focal length, f/4 imaging spectrometer (Acton 300i) with a 1200 g mm⁻¹ blazed grating. A slit width of 150 μm was used, resulting in 0.4 nm (FWHM) spectral resolution. The measured spectral range was 616.7–674.5 nm. Wavelength calibration for the spectrometer was obtained by observing a neon Penray lamp mounted on the inside of the observatory dome. The shape and line width of these emission lines also provided the instrument lineshape function, which was applied to the NO₃ reference spectra.

The spectrometer was equipped with a 1024 × 255, back-illuminated CCD detector temperature stabilized with circulating coolant. The pixel spacing of the CCD was 26 μm, which resulted in seven times oversampling of the instrument line width defined by the entrance slit projected on

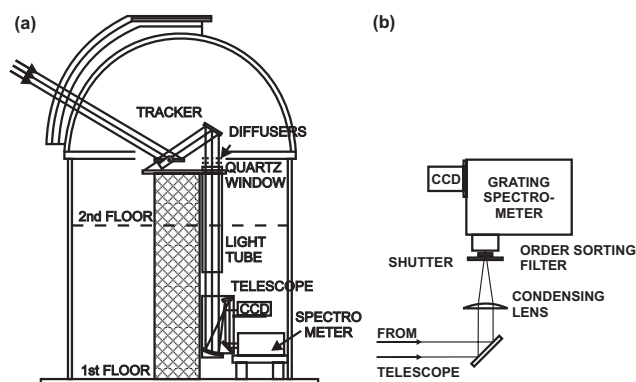


Fig. 1. Schematic of the instrument light path. **(a)** Light is collected by the primary of the heliostat (tracker), reflected down to the telescope on the first floor which conditions it to a 7 cm diameter collimated beam. **(b)** The light is then reflected to a condensing lens, past a shutter, order-sorting filter, and then into the spectrometer, recorded by a CCD.

the focal plane. For the initial observations, the CCD detector operated in imaging mode, with an integration time of three seconds at peak lunar intensity. The intensity of the moon decreases rapidly off full moon (50% decrease two days from full moon) and with increasing airmass, so the integration time was adjusted to maintain a constant CCD exposure level. Spectra, obtained between sunset and sunrise, were recorded every 10–20 min, yielding at least 30 column abundance values for each evening. To improve the signal-to-noise ratio, five scans were averaged to obtain a single archived spectrum. The five scans had the same integration time, but total integration time could differ when comparing averaged data on and off full moon. All spectra were dark-corrected, but not flat-fielded, since pixel-to-pixel variability canceled with comparison to the reference spectrum, as described below.

In the more recent datasets, June, August, and September of 2004, the collection frequency was increased to a spectrum every minute to improve the time resolution. This increased the number of column measurements to over 400 per night. To achieve this increased collection frequency, the detector was run in a mode that binned every 12 pixels along the spatial axis during data readout. In this case, 29 spectra were summed for each archived spectrum, with a total integration time of 7.25 s at peak lunar intensity.

2.2.2 Spectral analysis

Remote and in situ sensing of atmospheric NO₃ make use of the strong vibrational bands at 662 and 623 nm which are assigned to the (0,0) and (1,0) bands, respectively, of the ν_1 symmetric stretch in the $A^2E' \leftarrow X^2A_2'$ electronic transition (Ramsay, 1962). High resolution laboratory spectroscopy studies have shown these bands are diffuse with cross sec-

tions that are weakly dependent on temperature (Cantrell et al., 1987; Ravishankara and Mauldin, 1986; Sander, 1986; Yokelson et al., 1994) decreasing by 22% over the range of atmospheric temperatures from 220 K to 298 K. For ground-based remote sensing studies of NO₃, spectroscopic interferences with these bands include the O₂ gamma band at 628.8 nm, a broad O₄ band centered at 630 nm, and a weak water vapor band in the 640–665 nm spectral region. There is also an absorption band in this spectral range for NO₂, but the contribution from this band was negligible at Table Mountain. NO₂ has very weak lines in this spectral range that are lost in the noise for this measurement.

The spectrometer dispersion and grating position were selected to give a spectral bandpass of 616.7–674.5 nm. In this spectral interval we recorded and analyzed both the 623 and 662 nm absorption bands of NO₃. The spectra were analyzed using the differential optical absorption spectroscopy (DOAS) approach (Platt and Stutz, 2008) with the spectral analysis and deconvolution program, MFC (Stutz and Platt, 1996).

The principle of DOAS is to use only the high-frequency components of the spectrum to determine the quantity of an optically absorbing atmospheric component. The effect of the DOAS processing steps on the data is shown in Fig. 2. First, the slowly varying low frequency component of the background, from sources such as Rayleigh and Mie scattering effects and solar flux spectral variations, was removed numerically from the lunar occultation spectra. This was done by dividing the raw data with a smoothed version of the same data. Shown in Fig. 2b is the logarithm of this ratio, making the spectrum proportional to column abundance and molecular absorption cross section. The reflected solar Fraunhofer lines that dominate the raw spectra were then removed using solar reference spectra. The high-pass filtered lunar spectrum was divided by a high-pass filtered solar reference spectrum after aligning the spectra in wavelength with a nonlinear fit with stretch. The resulting spectrum was fit by least squares to high-pass filtered reference spectra of NO₃, H₂O, and O₂/O₄ (Fig. 2c). O₄ scales with the square of O₂ concentration, and therefore can be fit along with O₂.

The slant NO₃ column abundances calculated from the fit were converted to vertical column abundances by dividing by the airmass, a factor that describes the amount of air seen through a slant path in the atmosphere compared to a view directly overhead. The airmass was determined from the reciprocal of the cosine of the lunar zenith angle (a valid approximation for angles up to 80°) with an additional small correction for refraction.

To obtain the reference spectra for the solar features, we recorded direct solar spectra with two ground glass diffuser plates in the light path between the heliostat and telescope. The primary purpose of the diffuser plates was to average the observed radiance over the entire solar disk. Without the plates, only a small fraction of the solar disk was imaged onto the spectrometer slit, and the solar spectral features in the

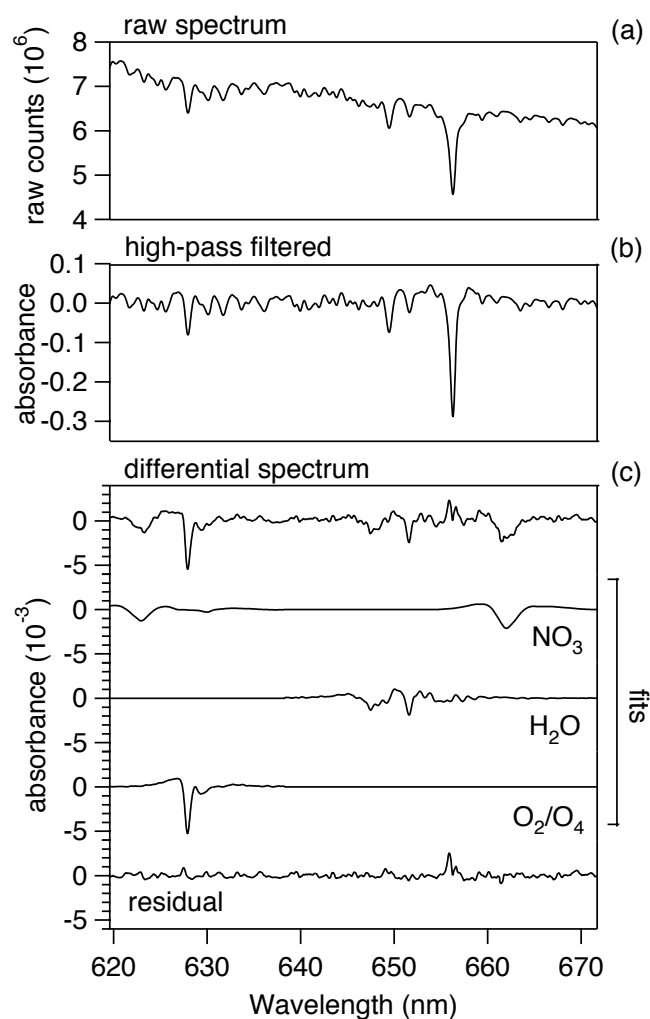


Fig. 2. Spectra at different stages of processing: (a) raw spectrum, with visibly sloping baseline, (b) high-pass filtered raw spectrum, created by dividing the raw spectrum with a smoothed version, and (c) the differential spectrum, after subtracting the solar reference spectrum (similar to (b)), with the individual fits for NO₃, water, O₂/O₄, and the resultant residual. The residual features result from errors in fitting the solar line.

non-diffuse spectra differed from those in the lunar spectra. With the diffuser plates, we regularly obtained RMS residual absorbances of less than 4×10^{-4} . The diffuser plates also helped to attenuate the solar beam, although additional neutral density filtering was used to avoid detector saturation.

Solar reference spectra were acquired over a day for the airmass range 1–7 (SZA 34–81°). New solar reference spectra were taken once a month during the time of the full moon datasets to account for small changes in instrument alignment. In addition to solar lines, these spectra contained terrestrial water vapor, O₂, and O₄ features with optical depths that were proportional to the airmass. The solar reference

spectrum used in the processing for a particular lunar spectrum had an airmass within ± 0.5 of the airmass of the lunar data, thereby removing much of the water, O₂, and O₄ column prior to additional processing. This intrinsically deals with saturation effects in the water vapor and oxygen spectra and provides an accurate representation of the spectra broadened by instrument line shape. In our experience, using water spectra from line-by-line radiative transfer models did not give the best residuals. Therefore to account for the remaining and variable water vapor and oxygen signals, we employed empirical reference spectra obtained from ratios of solar spectra at different airmasses. Since there is little overlap of the O₂/O₄ and water features, these two features were individually isolated and used as empirical spectral references. The low spectral resolution of measurement does not resolve individual lines for water and O₂, and therefore has little sensitivity to pressure broadening. The NO₃ reference spectra used were obtained from laboratory absorption cross section studies of NO₃ and have been measured over the temperature range relevant to the troposphere and stratosphere (Cantrell et al., 1987; Ravishankara and Mauldin, 1986; Ravishankara and Wine, 1983; Sander, 1986; Yokelson et al., 1994). The cross sections of Sander and Yokelson et al. are in excellent agreement over the range of overlap of temperature. Both studies observed a significant decrease in NO₃ cross sections at the peaks of the 662 and 623 nm bands with decreasing temperature. In contrast, the results of Cantrell et al. showed no dependence of cross section with temperature and are assumed to be incorrect. The results of Ravishankara and Mauldin disagree significantly with those of Yokelson et al. from the same group, and are assumed to be superseded by the latter. Although the temperature at the peak of the stratospheric NO₃ concentration profile at 40 km is roughly 260 K, the average temperature weighted by the model-predicted NO₃ concentration profile in the stratosphere is closer to 240 K. We have used the spectrum of Yokelson et al. at 240 K for the column retrievals presented here. Solomon et al. also used a reference temperature of 240 K, while Aliwell and Jones used 260 K.

2.2.3 Measurement uncertainty

The overall uncertainty for our measurement of total column NO₃ is approximately 17% RMS. The most important contributions to this uncertainty are systematic errors in cross section, and photon noise. The stated uncertainty in the NO₃ cross section is $\pm 10\%$ (Yokelson et al., 1994), excluding the errors associated with the temperature dependence of the cross sections. Our estimate of total column NO₃ assumes that the absorption is dominated by stratospheric contributions. There is a $\pm 6\%$ error associated with the use of a single cross section at a temperature of 240 K, if the temperature of the column actually varies between 220 K and 260 K. If there are contributions from tropospheric NO₃, the retrieved columns are a lower limit since the cross section of the band

peak at 662 nm for 298 K is 17% less than for 240 K. Photon noise in the system contributes an estimated 13% to the uncertainty. The detection limit for the NO₃ slant column abundance is 2×10^{12} molec cm⁻². The signal to noise ratio was >5 for most of the evening (during the steady state growth period); this ratio was larger for measurements through larger airmasses or larger NO₃ column amounts.

2.3 Long-path DOAS instrument

Horizontal column average measurements were made at TMF for August and September 2004 using a long-path differential optical absorption spectrometer (LP-DOAS). LP-DOAS is an active remote sensing technique that gives exceptionally low detection limits by averaging over a long (several kilometers) pathlength. Light from a broad-spectrum 500 W Xe arc lamp was collimated through a Newtonian telescope and broadcast to an array of corner-cube retroreflectors mounted on a radio tower located on the Blue Ridge in the Angeles National Forest. The distance between the instrument and the retroreflector array was approximately 3.4 km. Light incident on the retroreflector array traveled back through the atmosphere, was collected by the same telescope and transmitted through a fiber-optic cable to the spectrometer and detector. The difference in altitude between the LP-DOAS instrument and the tower-mounted retroreflector array was 298 m. A detailed description of the LP-DOAS instrument and the NO₃ analysis employed here is given in (Geyer et al., 1999). The measurement uncertainty of the LP-DOAS is dominated by the error in the absorption cross-section of NO₃, which is $\pm 10\%$ (Yokelson et al., 1994) as previously noted.

3 Model descriptions

3.1 1-D stratospheric model

A one-dimensional, photochemical steady state model of the stratosphere (Osterman et al., 1997) was run using TMF climatological profiles of temperature and O₃ as inputs, and the modeled NO₃ column abundances were compared to the TMF column measurements. The model calculates diurnally varying species concentrations, assuming each species reaches a balance between production and loss over 24 h for a given temperature and pressure profile and latitude. JPL 2006 cross sections and quantum yields were used to determine photolysis J-values, and JPL 2006 kinetic rate constants were used for reaction rates (Sander et al., 2006, 2003). Chemical inputs are profiles of O₃, H₂O, CH₄, NO_y, Cl_y, CO, H₂, C₂H₆, Br_y, and aerosol parameters based on a climatology derived from NASA satellite and balloon observations (e.g., Yang et al., 2006), as detailed in Table 1.

Additionally, SAGE III satellite measurements of O₃ in the stratosphere were used to verify the consistency between the 1-D stratospheric model and SAGE III measurements of

NO₃, testing the current understanding of stratospheric NO₃ chemistry (described in Appendix A). Analysis of the sensitivity of modeled NO₃ column to input parameters and to uncertainties of reaction rates were also conducted and are described in Appendix B.

3.1.1 Table mountain facility lidar climatology

Temperature and ozone concentration profiles have been measured at TMF by lidar since 1988 and offer a unique opportunity to compare our measurements with a model with realistic constraints. Temperature profiles were measured between 30–80 km and ozone profiles between 15–50 km, both with 300 m vertical resolution since September 1994 and with 600 m vertical resolution beforehand. Three cases were run using these data: climatological monthly mean values and variability of ozone concentration and temperature over the 10 year period 1988–1997 (data extracted from the published contour plots) (Leblanc and McDermid, 2000; Leblanc et al., 1998), and monthly mean profiles for 2003 and for 2004 provided by Leblanc (2005). Temperature and ozone profiles are sufficient for estimating the NO₃ column since NO₃ is primarily determined by these two quantities, as verified from a sensitivity study described in Appendix B1.

The change in NO₃ column at the extremes of variability was probed by running the model with both temperature and ozone variability added or subtracted from the climatological temperature and ozone profiles. The uncertainty in the climatological temperature measurements are 0.6 K at the middle of the altitude range, 8 K at 30 km, and <4 K at 80 km. The uncertainty of the climatological ozone measurements are a few percent at the peak of the ozone, 10–15% at 15 km, and more than 40% above 45 km. The uncertainty in ozone for the 2003 and 2004 monthly mean profiles was a minimum at 6% at the ozone peak, increasing in error above and below this altitude to 10% at 18 km and 42 km. The uncertainty in temperature for the 2003 and 2004 monthly mean profiles varied between 0.5 K and 1.3 K over 13–60 km.

The gaps in the ozone and temperature profiles were filled with the climatology from (1) the Upper Atmosphere Research Satellite (UARS) Reference Atmosphere Project (URAP) (Remedios et al., 2007; Wang et al., 1999; Randel et al., 1999), and then (2) a climatology dataset based on ozone data from Dütsch (1974) and ozone and temperature from the Middle Atmosphere Program (Barnett and Corney, 1985; Keating and Young, 1985), with adjustments to the ozone climatology based on in situ ozone measurements in the upper troposphere and lower stratosphere from many field programs. URAP is a compilation of global data from the CLAES, HALOE, HRDI, MLS and ISAMS instruments on the UARS satellite taken from April 1992 through seven years, processed into zonal monthly means with standard deviation. Two types of data were provided: “baseline” data obtained from April 1992 to March 1993, and “extended” datasets averaged over 7 years. We used extended data where

Table 1. Sources for the input parameters for each of the cases run on the 1-D stratospheric model.

Input parameter	Model run		
	TMF	SAGE III	sensitivity
temperature	TMF lidar data	From Sage III NO ₃ retrieval	URAP baseline dataset
O ₃	TMF lidar data	From Sage III NO ₃ retrieval	URAP extended dataset
H ₂ O	URAP, extended dataset		
CH ₄	URAP, extended dataset		
NO _y	Calculated from tracer relation Rinsland et al. (1999); Popp et al. (2001) using URAP N ₂ O baseline dataset		
Cl _y	Calculated from tracer relation from SOLVE data, using URAP N ₂ O baseline dataset		
CO	Static profile from MkIV flight Toon (1991); Sen et al. (1998)		
H ₂	Static profile based on measurements Dessler et al. (1994); Abbas et al. (1996); Rockmann et al. (2003)		
C ₂ H ₆	Static profile from MkIV flight Toon (1991); Sen et al. (1998)		
Br _y	Calculated from tracer relation (Wamsley et al. (1998) using URAP N ₂ O baseline dataset		
aerosol parameters	Monthly profiles from SAGE II aerosol measurements averaged over all years except those affected by the Pinatubo eruption Thomason et al. (1997)		

^a Gaps filled first with URAP data Remedios et al. (2007); Wang et al. (1999); Randel et al. (1999). For ozone, further gaps were filled by a climatology based on Dütsch (1974), on the Middle Atmosphere Project Keating and Young (1985), and from many in situ ozone measurements in the lower stratosphere and upper troposphere. For temperature, further gaps were filled from the Middle Atmosphere Project Barnett and Corney (1985).

^b URAP data is available averaged over 7 years (extended) or over 1992–1993 (baseline).

available. The ozone data used were from the extended time range, and the temperature data from the baseline time frame. We also used profiles of H₂O (extended), CH₄ (extended), and N₂O (baseline) from URAP. N₂O was used as a tracer to estimate model inputs for NO_y, Cl_y, and Br_y using well established tracer relations (e.g. Yang et al. (2006) and references therein).

Static profiles for CO and C₂H₆ from MkIV measurements (Toon, 1991; Sen et al., 1998), and a H₂ profile based on measurements in the stratosphere (Abbas et al., 1996; Dessler et al., 1994; Rockmann et al., 2003) were used for all months. Vertical profiles of sulfate aerosol surface area were based on zonal monthly mean measurements by SAGE II (Thomason et al., 1997) updated to include data acquired during the time of our NO₃ measurements.

3.2 GEOS-Chem tropospheric model

We use the GEOS-Chem global 3-D tropospheric chemistry and transport model (Bey et al., 2001; Park et al., 2004; Wu et al., 2007) to explore the spatial and temporal variability of NO₃ in the troposphere for a few days in August and September 2004, coinciding with our acquisition dates. The GEOS-Chem model (version 7.02.04, <http://www-as.harvard.edu/chemistry/trop/geos>) is driven by the assimilated meteorological GEOS-4 data from NASA Global Modeling and Assimilation Office (GMAO) with 6-hour temporal resolution (3-hour for surface variables and mixing depths) and a horizontal resolution of 1° × 1.25° with 55 layers in the vertical. The horizontal resolution of the GEOS-4 wind fields has been degraded to 2° × 2.5° for input into GEOS-Chem.

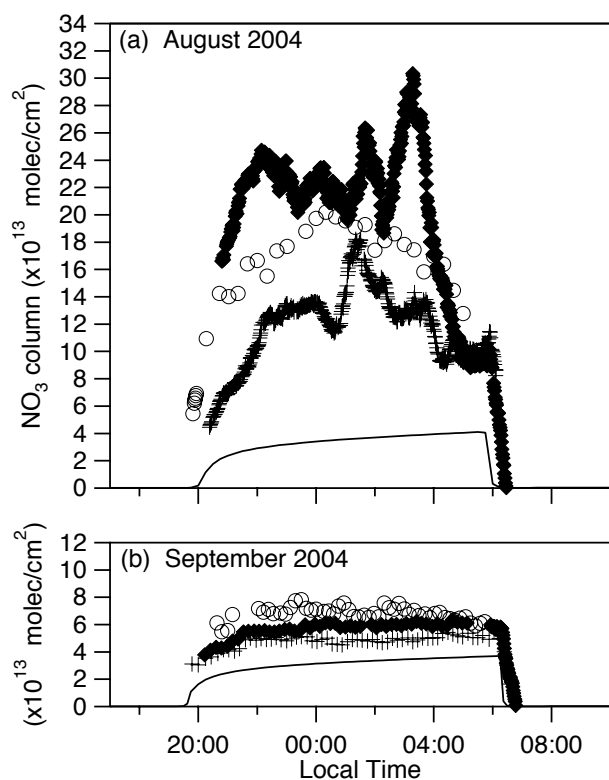


Fig. 3. Diurnal variation of NO₃ vertical column measured at Table Mountain, California for August and September 2004, along with calculated vertical columns from the 1-D stratospheric model (line). For August 2004 (a), three consecutive evenings of measurements are shown, the evenings of 28 August 2004 (open circle), 29 August 2004 (+), and 30 August 2004 (filled diamond). Also for September 2004 (b), three consecutive evenings of measurements are shown the evenings of 27 September 2004 (open circle), 28 September 2004 (+), and 29 September 2004 (filled diamond). The stratospheric model used monthly mean profiles from TMF lidar measurements from 2004 as input. Data from September, during the steady state nocturnal period, shows only every tenth point to avoid crowding the graph.

4 Results and discussion

4.1 Experimental results

As seen in model calculations in Fig. 3, the diurnal variation of stratospheric NO₃ can be characterized by four phases: daytime photolysis (negligible NO₃), sunset build-up (a rapid rise in NO₃ column), nocturnal steady state (a nearly linear, slow rise in NO₃ column), and sunrise destruction (rapid decrease in NO₃ column). These four stages were also observed in our measurements, except for some variations during the nocturnal steady state stage. Time series that monotonically increase, which occurs almost linearly during the steady state phase, are labeled as “model-like behavior” as seen in our measurements from September 2004 (Fig. 3b);

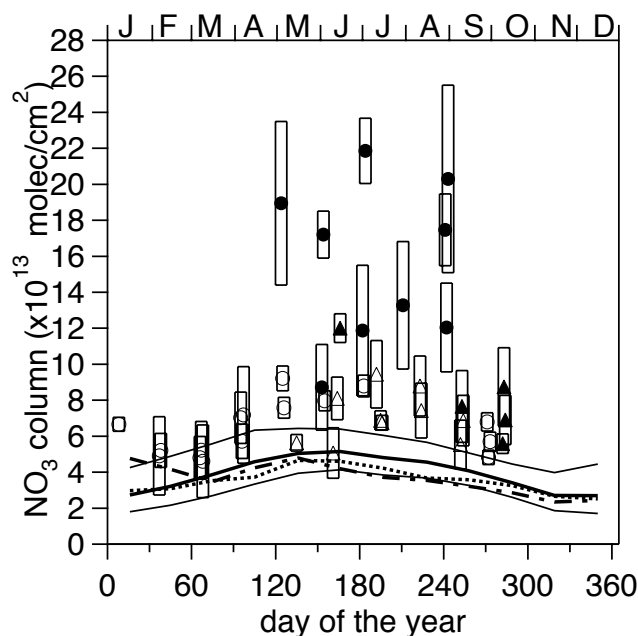


Fig. 4. Table Mountain Facility (TMF) NO₃ vertical column measurements compared to results from the 1-D photochemical model using TMF lidar profiles of ozone and temperature as inputs, plotted vs. day of year. Both the measured and modeled columns were averaged over the steady state portion of the night. The measured mean NO₃ columns shown are from 2003 (triangles)–2004 (circles); model-like and non-modeled behavior are denoted by open and filled symbols, respectively. The bars show the diurnal variability. The three cases run by the model are: the climatology from 1988–1997 along with the limits of the temperature and ozone variability taken from Leblanc et al. (Leblanc et al., 1998; Leblanc and McDermid, 2000), and mean profiles from Leblanc (Leblanc, 2005) for 2003 and 2004.

this label does not necessarily mean that these data are purely stratospheric in origin. The remaining data are described as “non-modeled behavior”, and displayed a wide variety of different temporal behavior with variability ranging from one to several hours, as seen in our measurements from August 2004 (Fig. 3a).

For purposes of comparison, each night of data was reduced to a time-averaged mean column and a standard deviation over the steady state phase, which was taken to be two hours after sunset up to roughly 30 min before sunrise. An annual plot of all the mean columns, with 2- σ standard deviations as error bars, is shown in Fig. 4. For 26 of the 40 days of analyzed data, the NO₃ columns followed model-like behavior (open symbols in Fig. 4). Within this subset of data a seasonal variation was observed, more clearly shown in Fig. 5. The NO₃ mean column averaged over summer months (April through September) was 7.5×10^{13} molec cm⁻². The column averaged over winter months (October through March) was 5.5×10^{13} molec cm⁻², as summarized in Table 2;

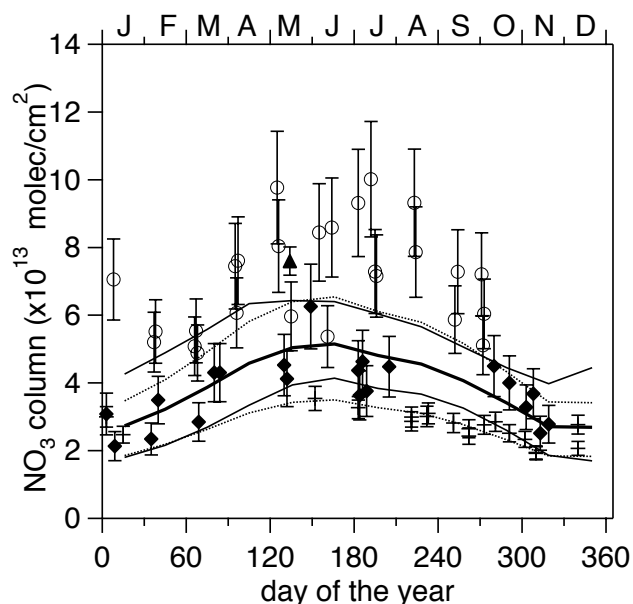


Fig. 5. Subset of the NO₃ vertical columns measured at Table Mountain Facility (TMF) that followed model-like behavior (open circle), data from Aliwell and Jones (filled triangle), Solomon et al. (1989) (filled diamond), and SAGE III satellite measurements (+) plotted versus day of year. These measurements are compared to a stratospheric photochemical 1-D model with temperature and ozone concentrations from a TMF climatology from 1988–1997 (thick line), along with the limits of the temperature and ozone variability (thin line) taken from Leblanc et al. (Leblanc et al., 1998; Leblanc and McDermaid, 2000). The uncertainty in the NO₃ column due to the uncertainty in the rate constants for N₂O₅ thermal decomposition, and reactions R1 and R2 are also shown in this figure (dotted line).

cloudy conditions limited the amount of data that could be acquired during winter and none was possible in 2003. We attribute the larger summertime values to a warmer atmosphere (both in the troposphere and stratosphere), which drives the thermal decomposition of N₂O₅ to form NO₂ and NO₃. In the 14 remaining cases with non-modeled behavior (closed symbols in Fig. 4), which occurred from May to early October, the range of mean columns was 6–22 × 10¹³ molec cm⁻² and the range of standard deviations was 1–5 × 10¹³ molec cm⁻². The low end of the range of standard deviations occurred for cases with relatively flat but decreasing temporal profiles, while the high end of the range was characterized by large oscillations in the NO₃ column.

The large oscillations in total column NO₃ that occurred over an evening did not originate from the stratosphere, since the primary source of variability in the stratosphere is from planetary waves, which have time scales longer than one day (Salby, 1984; Wu and Waters, 1996). Instead these variations are likely to arise from the troposphere. However, the complexity of mountain topography complicates the deter-

Table 2. Summary of NO₃ seasonal mean columns (in molecules cm⁻²) calculated for the subset of observations with “model-like behavior”, and for results from the 1-D stratospheric model using profiles from the lidar at TMF with monthly mean fields from 2003 and 2004 and ten year climatological inputs. There were no measurements during the October through March months in 2003. The standard deviation of the mean columns is shown in parentheses.

	April–September NO ₃ Mean Col (Std Dev)	October–March NO ₃ Mean Col (Std Dev)
Obs. (subset) 2003	7.5 (1.5) × 10 ¹³	–
Obs. (subset) 2004	7.5 (1.5) × 10 ¹³	5.5 (0.8) × 10 ¹³
Model (TMF 2003)	4.1 (0.5) × 10 ¹³	3.0 (0.4) × 10 ¹³
Model (TMF 2004)	3.9 (0.6) × 10 ¹³	3.3 (1.0) × 10 ¹³
Model (TMF climatology)	4.7 (0.4) × 10 ¹³	3.1 (0.5) × 10 ¹³

mination of the origin of the tropospheric air at TMF using traditional back trajectory methods. Depending on the movement of the air masses, we observed from a range of sources as diverse as desert air to polluted urban air and air from aloft due to mountain subsidence and drainage flow.

Model results by Lu and Turco (Lu and Turco, 1995, 1996; Lu et al., 2003) of the Los Angeles basin air flow give an idea of seasonal behavior during quiescent conditions. Their Surface Meteorology and Ozone Generation (SMOG) model calculates winds and tracer transport in the Los Angeles basin and surrounding mountain areas. Land warming by solar radiation propels onshore winds and upslope mountain flows during the day, with stronger winds in summer than winter. In the summer evenings, there are generally downslope flows from the mountains, and disorganized winds in the basin. Winter evenings have a stronger offshore component from radiative cooling of mountaintops and subsidence, driving the air towards the lower pressure off the coast. This suggests that daytime urban air is transported toward the mountains and over the passes year-round, but winter evenings are more efficient at flushing urban air from the mountains to the coast.

The two observed regimes for total column NO₃, model-like and non-modeled behavior, were consistent with the Lu and Turco analysis of local air flow. Between mid-October and April, when only model-like behavior was observed, there was little evidence for tropospheric contribution to the total column NO₃. In the summer, the daytime onshore component coupled with weakly organized evening flow would often lead to urban air being advected to the TMF site, resulting in large variations in detected NO₃. A signature of urban influence on column NO₃ was observed for 14 out of 31 days, for data collected between mid-April and mid-October in 2003 and 2004.

In Fig. 5, our model-like behavior data are shown compared to other measured column measurements using lunar occultation with grating spectrometers, from Solomon et al. (1989) and Aliwell and Jones (1996b). Data from Solomon et al. were taken from Fig. 10 of their paper and reduced by 18% to account for the updated NO₃ cross section of Yokelson et al. at 240 K, which was not available when the paper was published. The result of Aliwell and Jones and our data are in good agreement. While some of our data and that of Solomon et al. have overlapping error bars, the majority of their data is roughly $1\text{--}2 \times 10^{13}$ molec cm⁻² below the TMF columns. Solomon et al. confirmed most of their data was primarily stratospheric NO₃ by analyzing the dependence of the NO₃ slant column on the lunar zenith angle (LZA) near the horizon (LZA > 80°) (Solomon et al., 1989). A tropospheric NO₃ signal would grow much faster than the stratospheric NO₃ at high lunar zenith angles from slant path increases. We were not able to use this method to determine the tropospheric contribution because of pointing system view angles limited to less than 80°.

Surface concentration measurements of NO₃ were made with the UCLA LP-DOAS instrument during the August and September 2004 measurement periods. The results are shown along with the NO₃ column amounts measured by lunar occultation in Fig. 6. As shown in the figure, the short time-scale features in the 29–31 August LP-DOAS data are reproduced in the column data, implying a large boundary layer contribution to the column on those days. Some features seen in the column measurements were not present in the surface concentrations, which could be due to changing thickness of the polluted layer.

In contrast, data from 27–29 September 2004 had a much smaller contribution from the boundary layer. The LP-DOAS instrument confirmed that there were low NO₃ concentrations at the surface, as shown in Fig. 6. This period coincided with a Santa Ana wind event, characterized by a northerly downslope flow that advected dry desert air mixed with air from aloft over the measurement site. This circulation is driven by a high pressure system centered north of Southern California. This flow of air from the north over the mountains and through the passes to the LA basin drives wind speeds of 46 km h⁻¹ and gusts in excess of 90 km h⁻¹, carrying urban pollution offshore and away from Table Mountain Facility. Air quality measurements of surface NO₂, CO, and O₃ from Air Quality Management District (AQMD) stations (California Air Resources Board, 2007) in Victorville (14306 Park Avenue), Azusa, downtown Los Angeles (North Main Street), and west Los Angeles (Westchester Parkway), positioned progressively from the desert in Victorville towards the ocean, verifies that low concentrations of surface urban pollutants were found in the Mojave Desert and into Los Angeles County, and that the diurnal cycle for these chemicals was disrupted for this time period (see Fig. 7).

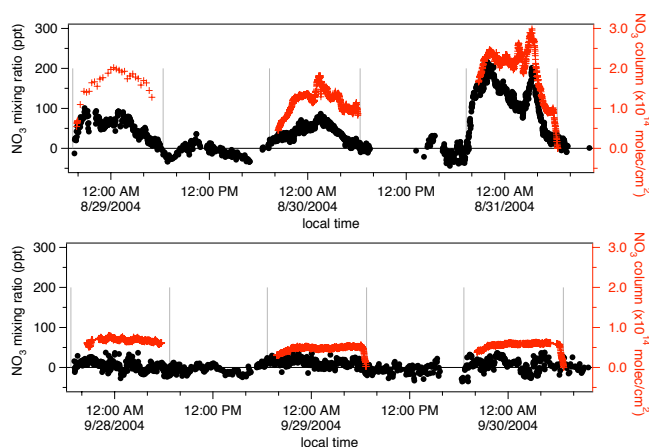


Fig. 6. Coincident measurements of NO₃ vertical column (in red) using lunar occultation and surface measurements of NO₃ concentration (in black) using long-path DOAS. Many of the large features in the data taken in August 2004 occur in both datasets. Measurements in September 2004 verify that there were very low levels of NO₃ concentration at the surface the whole evening.

4.2 Model results

4.2.1 Stratospheric model

Model results using averaged TMF temperatures over three different time periods are shown in Fig. 4: monthly averages from 2003, from 2004, and over a ten year period, 1988–1997. All three TMF model results exhibited a seasonal variability with higher values during the summer. Results from 2003 followed those of the ten-year average, with November through January having the lowest values of the year, and the highest values in April and May. Results from 2004 deviated from the other runs with larger modeled columns for January that decreased to climatological values from March onwards. The TMF seasonal averages for total column NO₃ are listed in Table 2.

4.2.2 Tropospheric model

From the results of the GEOS-Chem 3-D chemical transport model, we investigated the expected range of tropospheric NO₃ column abundances for specific geographic regions. GEOS-Chem could not be used for quantitative comparisons with TMF observations since the grid size is too large to resolve the local meteorology and the detailed transport of pollution from the LA Basin. In order to understand the range of the expected NO₃ variability from the model, column abundances are compared for three different locations: TMF (mountainous region with nearby urban pollution sources, 33–35° N, 241.25–243.75° E), western Colorado (northern midlatitude mountain area, 37–41° N, 251.25–253.75° E), and the northern midlatitude Pacific Ocean (no urban sources

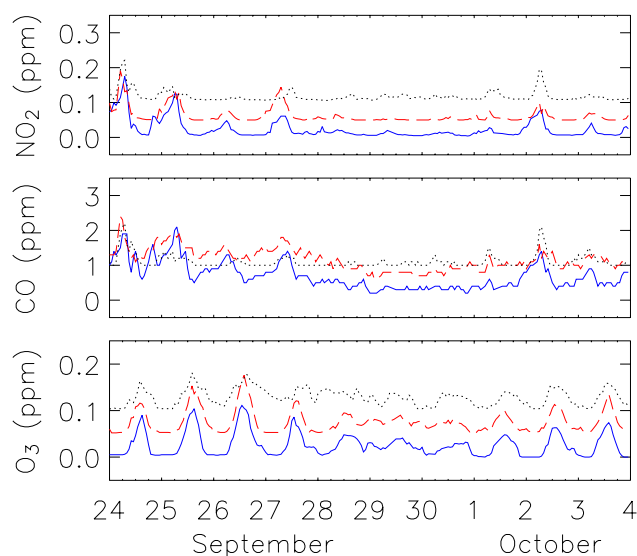


Fig. 7. Time series data for NO₂, CO, and O₃ mixing ratio (offset progressively by 0.05 ppm) at three AQMD monitoring sites located in the Mojave Desert and progressively towards Los Angeles: Victorville (black dot), Azusa (red dash), and downtown Los Angeles (blue solid). The Santa Ana winds occurred 28–30 September 2004, evidenced by the disturbance of the diurnal cycle and lower diurnal concentrations. The date labels correspond to 00:00 for each day.

or orographic influences, 29–45° N, 178.75–228.75° E). In addition, we calculate the NO₃ column for the northern midlatitude zonal mean (29–45° N). The regions were compared for six evenings that coincide with data collection (the evenings of 28–30 August 2004 and 27–29 September 2004). Total columns as well as the partial columns from the boundary layer and free troposphere were calculated.

The boundary layer defined by the model for each time step was not used since the boundary layer is shallower during night time and does not reflect the pollution that was distributed throughout the boundary layer in the daytime. Instead, a column was constructed by setting the boundary to the maximum thickness of the boundary layer for that day. This column is labeled as the “thickest boundary layer”, with the difference of the total with this quantity labeled as the “thinnest free troposphere”.

The time evolution of tropospheric NO₃, shown in Fig. 8 and Fig. A1, varied over the different regions but in most cases there was a sawtooth pattern not unlike that for the stratosphere: daytime photolysis with negligible NO₃, a nearly linear rise in NO₃ column over the evening followed by a rapid decrease in NO₃ column at sunrise. The thickest boundary layer column tended to mimic the total column shape, but for all cases the thinnest free tropospheric column consistently had the sawtooth pattern.

The diurnal averages, calculated with the same method as with the measurements, are summarized in Table 3. The

Table 3. Mean, median, and standard deviation of column NO₃ from the GEOS-Chem 3-D global transport and chemistry model for the evenings of 28–30 August 2004 and 27–29 September 2004, which coincide with data collection days. Four regions were investigated, Los Angeles (contains TMF), northern midlatitude Pacific, western Colorado, and the northern midlatitude band (30–45° N). The columns are calculated as total, the column below the maximum extent of the boundary layer for the previous day, and the column above.

	NO ₃ Mean Column ($\times 10^{13}$ cm ⁻²)					
	Los Angeles			N midlat Pacific		
	Total	BL*	FT*	Total	BL*	FT*
28 August 2004	71	73	13	5.6	0.018	5.6
29 August 2004	69	59	10	5.3	0.015	5.3
30 August 2004	73	64	9.3	5.2	0.015	5.2
27 September 2004	54	48	5.5	4.7	0.033	4.7
28 September 2004	34	28	5.4	5.0	0.051	5.0
29 September 2004	16	10	5.7	5.0	0.097	4.9
	Western Colorado			Northern midlatitude band		
	Total	BL*	FT*	Total	BL*	FT*
	28 August 2004	4.3	3.3	1.1	9.6	3.3
29 August 2004	5.7	4.7	1.0	9.0	2.9	6.1
30 August 2004	7.0	6.0	0.95	8.9	2.9	6.0
27 September 2004	4.5	3.5	1.1	9.7	3.8	5.8
28 September 2004	4.5	2.4	2.1	9.4	3.4	6.0
29 September 2004	2.9	1.9	0.98	11	3.8	6.8

model grid cell over Los Angeles has large tropospheric NO₃ columns from anthropogenic NO_x with roughly 20–70 $\times 10^{13}$ molec cm⁻², while the data at a midlatitude mountainous region (western Colorado) and without nearby urban sources (northern midlatitude Pacific) had significantly smaller tropospheric columns (4–5 $\times 10^{13}$ molec cm⁻²). The thinnest free tropospheric column was at its lowest over the mountain region, (1 $\times 10^{13}$ molec cm⁻²). The midlatitude zonal mean value is 6 $\times 10^{13}$ molec cm⁻². These values are consistent with the difference between our TMF measurements of total column NO₃ and model amounts of stratospheric partial column NO₃. As discussed below, this suggests that NO₃ in the free troposphere can regenerate each evening to substantial concentrations over a series of days, indistinguishable from stratospheric NO₃ based solely on the time evolution (diurnal variation) of the measured signal. This indicates a lack of chemical loss of NO_x and a high oxidation capacity in the upper troposphere.

4.3 Model and measurement comparison

The measured NO₃ columns along with results from 1-D stratospheric model constrained by measured temperatures and ozone concentrations from TMF showed a seasonal trend with higher NO₃ in the summer months. Measurements

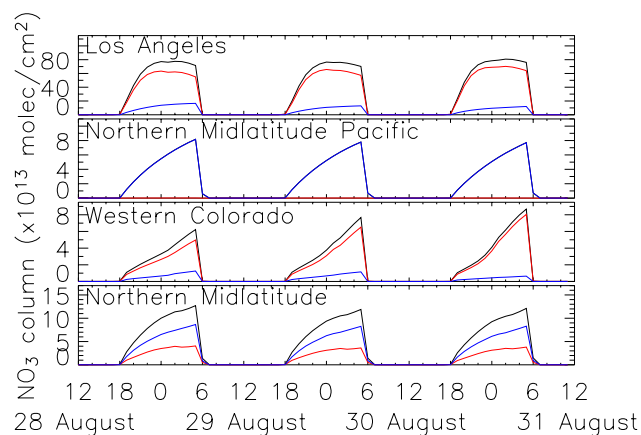


Fig. 8. Time evolution of total tropospheric vertical column (black), “thickest boundary layer” vertical column (red), and “thinnest free tropospheric” vertical column (blue) as calculated from 3-D global chemical transport model GEOS-Chem, for four different regions during three days in August. The “thickest boundary layer” column for an evening is the column calculated from the surface to the height of the maximum thickness boundary layer from the preceding day. The thinnest free troposphere is the difference between the total tropospheric column and the thickest boundary layer. The four regions are Los Angeles (33–35° N, 241.25–243.75° E), western Colorado (37–41° N, 251.25–253.75° E), the northern midlatitude Pacific Ocean (29–45° N, 178.75–228.75° E), and in the northern midlatitude band (29–45° N).

and model results from January–March 2004 were consistent within error bars as seen in Fig. 4, even duplicating the decrease in mean NO₃ column over these months not seen in the other model results. However, as seen in Table 2, the measured data are consistently larger than the modeled data by over 2×10^{13} molec cm⁻² for both summer and winter averages. This suggests that there is significant NO₃ in the troposphere; the stratospheric model correlated well with measured stratospheric NO₃ columns from SAGE III, as discussed in Appendix A, therefore we believe the model is reliable.

While it is clear that our NO₃ columns exhibiting non-modeled behavior have contributions from the boundary layer, even days with established low surface NO₃ concentrations, such as 27–30 September 2004 (Fig. 3b), had mean columns of NO₃ that were on average 2×10^{13} molec cm⁻² more than the model amount. Low levels of NO₃ were detected by LP-DOAS in September, but the measured columns were still on average 2×10^{13} molec cm⁻² greater than the modeled column, which is more NO₃ than a uniform troposphere with 3 ppt of NO₃, the detection limit of the instrument. Other measurements have determined there can be significantly larger concentrations of NO₃ above the surface in the upper boundary layer and lower free troposphere, using zenith sky measurements at sunrise compared to sur-

face DOAS measurements (Allan et al., 2002). GEOS-Chem results for the northern midlatitude band (29–45° N) for the six days in August and September 2004 highlighted in this study found that the average thinnest free tropospheric column was 6×10^{13} molec cm⁻² while the average thickest boundary layer column was 3×10^{13} molec cm⁻². For this case, significant NO₃ existed in the free troposphere with smoothly varying diurnal variation that is indistinguishable from modeled stratospheric NO₃ diurnal variation. This result indicates there is a sizable contribution to the column of NO₃ from the troposphere above the boundary layer. Brown et al. (2007a) reached similar conclusions based on aircraft measurements over the east coast of the United States.

5 Conclusions

We have measured the diurnal variation of the NO₃ column over Table Mountain Facility, California (34.4° N, 117.7° W), using ground-based visible absorption spectroscopy of moonlight. We observed two sets of behavior during the steady state phase of the evening: one described as “model-like behavior” followed the expected slow linear increase (mean columns of $5\text{--}9 \times 10^{13}$ molec cm⁻² for 26 out of 40 days), and the other, called “non-modeled behavior”, showed large departures from model behavior, often correlated with large mean NO₃ columns ($6\text{--}22 \times 10^{13}$ molec cm⁻² over 14 out of 40 days) and large standard deviations (up to 5×10^{13} molec cm⁻²), mostly during May through early October. The changes in NO₃ column seen in the non-modeled data are not likely due to variability in the stratosphere and are attributed to boundary layer sources.

Comparison to results from a 1-D photochemical model with temperature and ozone profiles taken from onsite lidar instruments showed that for the most part we measured more NO₃ than found using the model. The model compares well with stratospheric column NO₃ reported by SAGE III. These comparisons suggest significant contributions to total column NO₃ from the free troposphere at all times, with the tropospheric contribution exhibiting a diurnal pattern similar to the stratospheric column. This is supported by simultaneous surface measurements with LP-DOAS in September 2004, and results from the global tropospheric chemical and transport model, GEOS-Chem. This indicates that the upper troposphere has similar chemical processes and characteristics as the stratosphere.

Appendix A

The SAGE III (Meteor-3M) instrument (SAGE III ATBD, 2002) retrieved NO₃ concentration profiles from 20–60 km and O₃ concentration profiles from 15–50 km by satellite lunar occultation at moonset or moonrise. The retrieval process used temperature and pressure profiles from meteorological

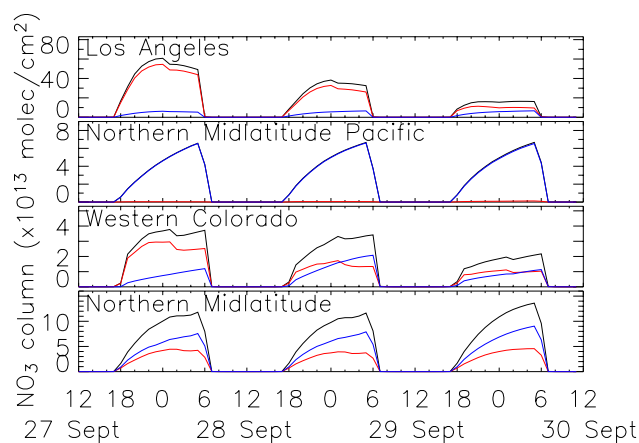


Fig. A1. Same as Fig. 8 except for September.

data from the National Centers for Environmental Prediction (NCEP) (Kalnay et al., 1996). These NCEP temperature and pressure profiles along with the SAGE III retrieved O₃ profiles were used as inputs for the stratospheric model and the resulting modeled NO₃ columns were compared with SAGE III NO₃ measurements. Available data spans from May 2002 to October 2005 (the mission was terminated March 2006), and 1184 data points from the latitude band between -70 and 70° were used; local times of the measurements were between 22:00–02:00.

The 1-D stratospheric model described in the paper was run with inputs from SAGE III lunar O₃ measurements as well as the temperature and pressure data from NCEP reanalysis used in the SAGE III retrievals. The O₃ profile below 15 km and above 50 km was filled with a climatology based on Dütsch and the Middle Atmosphere Project, described in the model description in the body of the paper; this has little impact on the scientific interpretation of our results, since the altitude range of interest for NO₃ is covered by the SAGE III measurements. The rest of the chemical inputs were the same as described for the TMF model runs.

The NO₃ profiles were integrated over the 18–60 km altitude range to determine a stratospheric partial NO₃ column comparable to the one calculated from SAGE III data. These columns were further reduced to a mean column and standard deviation calculated over the nocturnal steady state period, as done with our measurements.

The modeled stratospheric NO₃ columns are plotted against the values derived from integration of the SAGE III NO₃ vertical profiles in Fig. A2. The bulk of the data points cluster along the one-to-one line. Since both sets of data have significant uncertainties, we used a linear fit that considered both x and y errors (the details are described in Wang et al., 2008), rather than a standard linear fit that considers only errors in y . The uncertainty in the modeled NO₃ column due to uncertainties in input temperature

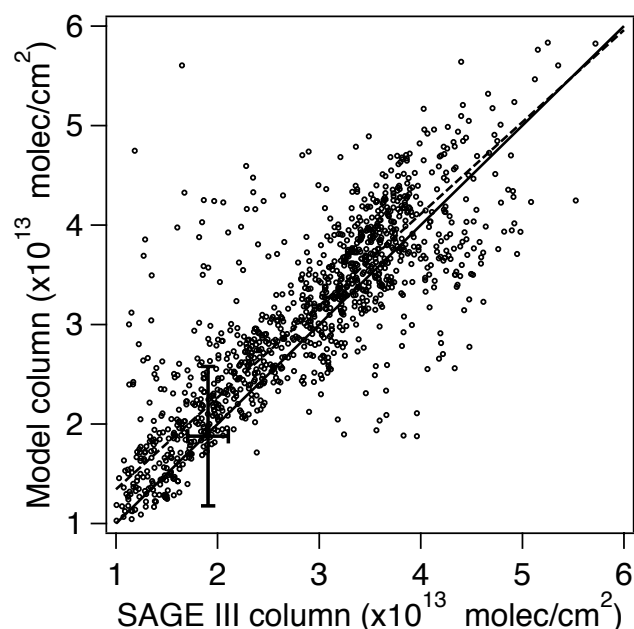


Fig. A2. Modeled NO₃ vertical columns using SAGE III lunar profiles as model input, compared to the SAGE III measured NO₃ columns within a band from 70° S to 70° N. The one-to-one line is shown as a solid line, and a linear fit to the data (with a slope of 0.92) is shown as a dashed line. The uncertainty in the SAGE III NO₃ column (2×10^{12} molec cm⁻²) and the uncertainty in the modeled column (7×10^{12} molec cm⁻²) are shown on one data point.

and O₃ profiles was estimated to be 0.7×10^{13} molec cm⁻², and uncertainty in the measured NO₃ column derived from the quoted uncertainties in the SAGE III NO₃ retrieved profiles was 0.2×10^{13} molec cm⁻². This resulted in a linear fit with a slope of 0.92 ± 0.02 and an intercept of 0.42×10^{13} molec cm⁻², with a reduced Chi squared, χ_{red}^2 , of 4.3. The reduced Chi squared is the χ^2 statistic normalized by the degrees of freedom, with a value of one indicative of a good fit (residual of fit and data is same order as errors), much less than one an indication of overestimated errors, and much greater than one of underestimated errors. From these fit results we assert that the modeled stratospheric NO₃ columns are consistent with the SAGE III measured columns.

Appendix B

B1 Sensitivity study of modeled NO₃ on input parameters in 1-D stratospheric model

We conducted a sensitivity study of the 1-D stratospheric model to determine to which input parameters the NO₃ column was most sensitive. Changes of $\pm 5\%$ concentration or ± 5 K were applied to the entire vertical profile of an individual input parameter. These changes were applied to

Table B1. Summary of sensitivity coefficients due to variations in temperature, ozone, and relevant reaction rate constants. Temperature was varied by ± 5 K, ozone by $\pm 5\%$, NO_y by $\pm 5\%$, and the rate constants were varied by their quoted error limits (Sander et al., 2003).

	Sensitivity coefficients	
	Negative variation	Positive variation
Temperature (5 K)	-0.25	0.36
O ₃ (5%)	-0.05	0.05
NO _y (5%)	-0.01	0.01
NO ₂ + O ₃ → NO ₃ + O ₂	-0.24	0.29
N ₂ O ₅ → NO ₃ + NO ₂	-0.04	0.06
NO ₃ + NO ₂ + M ↔ N ₂ O ₅ + M	0.12	-0.12

atmospheric profiles using the URAP climatology for all twelve months. Other chemical profiles not provided by URAP used the same sources as described for the TMF model runs.

We found that out of the various input parameters to the 1-D model, the NO₃ column is most sensitive to temperature and O₃. An increase or decrease of temperature by 5 K in the model resulted in change in the mean NO₃ column by 36% or -25%, respectively. A linear response was observed below 30 km; from 30–45 km a strongly nonlinear response was observed. A change of $\pm 5\%$ in the ozone concentration resulted in a change in the mean NO₃ column by $\pm 5\%$, with no altitude dependence in the sensitivity from 18–50 km. This directly proportional, linear relationship between NO₃ and ozone concentration occurs when NO₃ concentration is in steady state. NO_y also had a small effect, with the $\pm 5\%$ change in NO_y concentration resulting in a $\pm 1\%$ change in the NO₃ column. The effect on NO₃ from changes in the input concentration of other chemicals was negligible. These sensitivity coefficients are summarized in Table B1.

B2 Error propagation of reaction rates to NO₃ columns

Sensitivity of the NO₃ column to the errors in the rates of reactions relevant to NO₃ concentration was probed. The reaction rates of NO₃ creation from NO₂ + O₃ (R1), thermal decomposition of N₂O₅, and N₂O₅ formation (R2), were individually changed by their quoted error (Sander et al., 2003) for the SAGE III runs described in the model description, section 3.1. The sensitivity coefficients are summarized in Table B1. The greatest sensitivity of the NO₃ column to reaction rate errors was found for the NO₃ formation reaction from NO₂ + O₃. The root-mean-square variation for all rate changes that increase NO₃ was 27%, and 32% for changes that decrease NO₃ column. These percent changes were ap-

plied to the TMF climatology and are plotted as the pair of dotted lines in Fig. 5. The plotted range of NO₃ columns due to reaction rate errors was of similar magnitude as the range of NO₃ values calculated from the variability observed by the TMF lidar.

Acknowledgements. The research described in this paper was carried out at Jet Propulsion Laboratory, California Institute of Technology. It was supported by grants from the National Aeronautics and Space Administration. The SAGE III data used in this comparison are from L2 Lunar Event Species Profiles, v3.00, available from the NASA Langley Research Center Atmospheric Sciences Data Center (<http://eosweb.larc.nasa.gov>). We thank R. Moore for assistance with the SAGE III data, T. Leblanc for the TMF lidar data, Atmospheric and Environmental Research for use of LBLRTM, and S. Wang and A. Lambert for the orthogonal linear fit program. We also thank D. Natzic for technical assistance, L. Kovalenko for assistance with the photochemical model, and H. Bösch for discussions and calculations on atmospheric scattering. Others who have made significant technical and discussion contributions include R. Lu, D. Wu, G. Mount, V. Nemtchinov, and D. Peterson.

Edited by: J. B. Burkholder

References

- Abbas, M. M., Gunson, M. R., Newchurch, M. J., Michelsen, H. A., Salawitch, R. J., Allen, M., Abrams, M. C., Chang, A. Y., Goldman, A., Irion, F. W., Moyer, E. J., Nagaraju, R., Rinsland, C. P., Stiller, G. P., and Zander, R.: The hydrogen budget of the stratosphere inferred from ATMOS measurements of H₂O and CH₄, *Geophys. Res. Lett.*, 23, 2405–2408, 1996.
- Aldener, M., Brown, S. S., Stark, H., Williams, E. J., Lerner, B. M., Kuster, W. C., Goldan, P. D., Quinn, P. K., Bates, T. S., Fehsenfeld, F. C., and Ravishankara, A. R.: Reactivity and loss mechanisms of NO₃ and N₂O₅ in a polluted marine environment: Results from in situ measurements during New England Air Quality Study 2002, *J. Geophys. Res.-Atmos.*, 111, D23S73, doi:10.1029/2006JD007252, 2006.
- Aliwell, S. R. and Jones, R. L.: Measurement of atmospheric NO₃ 1. Improved removal of water vapour absorption features in the analysis for NO₃, *Geophys. Res. Lett.*, 23, 2585–2588, 1996a.
- Aliwell, S. R. and Jones, R. L.: Measurement of atmospheric NO₃ 2, Diurnal variation of stratospheric NO₃ at midlatitude, *Geophys. Res. Lett.*, 23, 2589–2592, 1996b.
- Aliwell, S. R. and Jones, R. L.: Measurements of tropospheric NO₃ at midlatitude, *J. Geophys. Res.-Atmos.*, 103, 5719–5727, 1998.
- Allan, B. J., McFiggans, G., Plane, J. M. C., Coe, H., and McFadyen, G. G.: The nitrate radical in the remote marine boundary layer, *J. Geophys. Res.-Atmos.*, 105, 24191–24204, 2000.
- Allan, B. J., Plane, J. M. C., Coe, H., and Shillito, J.: Observations of NO₃ concentration profiles in the troposphere, *J. Geophys. Res.-Atmos.*, 107, 4588, doi:10.1029/2002JD002112, 2002.
- Ambrose, J. L., Mao, H., Mayne, H. R., Stutz, J., Talbot, R., and Sive, B. C.: Nighttime nitrate radical chemistry at Appledore island, Maine during the 2004 international consortium for atmospheric research on transport and transformation, *J. Geophys. Res.-Atmos.*, 112, D21302, doi:10.1029/2007JD008756, 2007.

- Ameekudzi, L. K., Sinnhuber, B. M., Sheode, N. V., Meyer, J., Rozanov, A., Lamsal, L. N., Bovensmann, H., and Burrows, J. P.: Retrieval of stratospheric NO₃ vertical profiles from SCIAMACHY lunar occultation measurement over the Antarctic, *J. Geophys. Res.-Atmos.*, 110, D20304, doi:10.1029/2004JD005748, 2005.
- Atkinson, R.: Kinetics and Mechanisms of the Gas-Phase Reactions of the NO₃ Radical with Organic-Compounds, *J. Phys. Chem. Ref. Data*, 20, 459–507, 1991.
- Ayers, J. D. and Simpson, W. R.: Measurements of N₂O₅ near Fairbanks, Alaska, *J. Geophys. Res.-Atmos.*, 111, D14309, doi:10.1029/2006JD007070, 2006.
- Barnett, J. J. and Corney, M.: Middle atmosphere reference model derived from satellite data, Middle Atmosphere Program: Handbook for MAP Volume 16, SCOSTEP Secretariat, Univ of Illinois, Urbana, 1985.
- Bey, I., Jacob, D. J., Yantosca, R. M., Logan, J. A., Field, B. D., Fiore, A. M., Li, Q. B., Liu, H. G. Y., Mickley, L. J., and Schultz, M. G.: Global modeling of tropospheric chemistry with assimilated meteorology: Model description and evaluation, *J. Geophys. Res.-Atmos.*, 106, 23073–23095, 2001.
- Brown, S. S., Stark, H., Ryerson, T. B., Williams, E. J., Nicks, D. K., Trainer, M., Fehsenfeld, F. C., and Ravishankara, A. R.: Nitrogen oxides in the nocturnal boundary layer: Simultaneous in situ measurements of NO₃, N₂O₅, NO₂, NO, and O₃, *J. Geophys. Res.-Atmos.*, 108, 4299, doi:10.1029/2002JD002917, 2003.
- Brown, S. S., Dibb, J. E., Stark, H., Aldener, M., Vozella, M., Whitlow, S., Williams, E. J., Lerner, B. M., Jakoubek, R., Middlebrook, A. M., DeGouw, J. A., Warneke, C., Goldan, P. D., Kuster, W. C., Angevine, W. M., Sueper, D. T., Quinn, P. K., Bates, T. S., Meagher, J. F., Fehsenfeld, F. C., and Ravishankara, A. R.: Nighttime removal of NO_x in the summer marine boundary layer, *Geophys. Res. Lett.*, 31, L07108, doi:10.1029/2004GL019412, 2004.
- Brown, S. S., Dube, W. P., Osthoff, H. D., Stutz, J., Ryerson, T. B., Wollny, A. G., Brock, C. A., Warneke, C., De Gouw, J. A., Atlas, E., Neuman, J. A., Holloway, J. S., Lerner, B. M., Williams, E. J., Kuster, W. C., Goldan, P. D., Angevine, W. M., Trainer, M., Fehsenfeld, F. C., and Ravishankara, A. R.: Vertical profiles in NO₃ and N₂O₅ measured from an aircraft: Results from the NOAA P-3 and surface platforms during the New England Air Quality Study 2004, *J. Geophys. Res.-Atmos.*, 112, D22304, doi:10.1029/2007JD008883, 2007a.
- Brown, S. S., Dubé, W. P., Osthoff, H. D., Wolfe, D. E., Angevine, W. M., and Ravishankara, A. R.: High resolution vertical distributions of NO₃ and N₂O₅ through the nocturnal boundary layer, *Atmos. Chem. Phys.*, 7, 139–149, doi:10.5194/acp-7-139-2007, 2007b.
- Cageao, R. P., Blavier, J.-F., McGuire, J. P., Jiang, Y., Nemtchinov, V., Mills, F. P., and Sander, S. P.: High-resolution Fourier-transform ultraviolet-visible spectrometer for the measurement of atmospheric trace species: application to OH, *Appl. Optics*, 40, 2024–2030, 2001.
- California Air Resources Board: 2007 Air Quality Data DVD, 2007.
- Cantrell, C. A., Davidson, J. A., Shetter, R. E., Anderson, B. A., and Calvert, J. G.: The temperature invariance of the NO₃ absorption cross-section in the 662-nm region, *J. Phys. Chem.*, 91, 5858–5863, 1987.
- Carslaw, N., Carpenter, L. J., Plane, J. M. C., Allan, B. J., Burgess, R. A., Clemmshaw, K. C., Coe, H., and Penkett, S. A.: Simultaneous observations of nitrate and peroxy radicals in the marine boundary layer, *J. Geophys. Res.-Atmos.*, 102, 18917–18933, 1997a.
- Carslaw, N., Plane, J. M. C., Coe, H., and Cuevas, E.: Observations of the nitrate radical in the free troposphere at Izana de Tenerife, *J. Geophys. Res.-Atmos.*, 102, 10613–10622, 1997b.
- Coe, H., Allan, B. J., and Plane, J. M. C.: Retrieval of vertical profiles of NO₃ from zenith sky measurements using an optimal estimation method, *J. Geophys. Res.-Atmos.*, 107, 4587–4600, 2002.
- Dessler, A. E., Weinstock, E. M., Hints, E. J., Anderson, J. G., Webster, C. R., May, R. D., Elkins, J. W., and Dutton, G. S.: An Examination Of The Total Hydrogen Budget Of The Lower Stratosphere, *Geophys. Res. Lett.*, 21, 2563–2566, 1994.
- Dütsch, H. U.: Ozone Distribution In Atmosphere, *Can. J. Chem.*, 52, 1491–1504, 1974.
- Geyer, A. and Platt, U.: Temperature dependence of the NO₃ loss frequency: A new indicator for the contribution of NO₃ to the oxidation of monoterpenes and NO_x removal in the atmosphere, *J. Geophys. Res.-Atmos.*, 107, 4431, doi:10.1029/2001JD001215, 2002.
- Geyer, A., Alicke, B., Mihelcic, D., Stutz, J., and Platt, U.: Comparison of tropospheric NO₃ radical measurements by differential optical absorption spectroscopy and matrix isolation electron spin resonance, *J. Geophys. Res.-Atmos.*, 104, 26097–26105, 1999.
- Geyer, A., Alicke, B., Konrad, S., Schmitz, T., Stutz, J., and Platt, U.: Chemistry and oxidation capacity of the nitrate radical in the continental boundary layer near Berlin, *J. Geophys. Res.-Atmos.*, 106, 8013–8025, 2001.
- Geyer, A., Alicke, B., Ackermann, R., Martinez, M., Harder, H., Brune, W., di Carlo, P., Williams, E., Jobson, T., Hall, S., Shetter, R., and Stutz, J.: Direct observations of daytime NO₃: Implications for urban boundary layer chemistry, *J. Geophys. Res.-Atmos.*, 108, 4368, doi:10.1029/2002JD002967, 2003.
- Hapke, B. W., Nelson, R. M., and Smythe, W. D.: The Opposition Effect of the Moon—the Contribution of Coherent Backscatter, *Science*, 260, 509–511, 1993.
- Hauchecorne, A., Bertaux, J. L., Dalaudier, F., Cot, C., Lebrun, J. C., Bekki, S., Marchand, M., Kyrola, E., Tamminen, J., Sofieva, V., Fussen, D., Vanhellefont, F., d'Andon, O. F., Barrot, G., Mangin, A., Theodore, B., Guirlet, M., Snoeij, P., Koopman, R., de Miguel, L. S., Fraisse, R., and Renard, J. B.: First simultaneous global measurements of nighttime stratospheric NO₂ and NO₃ observed by Global Ozone Monitoring by Occultation of Stars (GOMOS)/Envisat in 2003, *J. Geophys. Res.-Atmos.*, 110, D18301, doi:10.1029/2004JD005711, 2005.
- Kalnay, E., Kanamitsu, M., Kistler, R., Collins, W., Deaven, D., Gandin, L., Iredell, M., Saha, S., White, G., Woollen, J., Zhu, Y., Chelliah, M., Ebisuzaki, W., Higgins, W., Janowiak, J., Mo, K. C., Ropelewski, C., Wang, J., Leetmaa, A., Reynolds, R., Jenne, R., and Joseph, D.: The NCEP/NCAR 40-year reanalysis project, *B. Am. Meteorol. Soc.*, 77, 437–471, 1996.
- Keating, G. M. and Young, D. F.: Interim reference ozone models for the middle atmosphere, Middle Atmosphere Program: Handbook for MAP Volume 16, SCOSTEP Secretariat, University of Illinois, Urbana, 1985.

- Lal, M., Sidhu, J. S., Das, S. R., and Chakrabarty, D. K.: Atmospheric NO₃ observations over low-latitude northern-hemisphere during night, *J. Geophys. Res.-Atmos.*, 98, 23029–23037, 1993.
- Leblanc, T.: unpublished data, 2005.
- Leblanc, T. and McDermid, I. S.: Stratospheric ozone climatology from lidar measurements at Table Mountain (34.4° N, 117.7° W) and Mauna Loa (19.5° N, 155.6° W), *J. Geophys. Res.-Atmos.*, 105, 14613–14623, 2000.
- Leblanc, T., McDermid, I. S., Keckhut, P., Hauchecorne, A., She, C. Y. and Krueger, D. A.: Temperature climatology of the middle atmosphere from long-term lidar measurements at middle and low latitudes, *J. Geophys. Res.-Atmos.*, 103, 17191–17204, 1998.
- Li, S. W., Liu, W. Q., Xie, P. N., Li, A., Qin, M., Peng, F. M., and Zhu, Y. W.: Observation of the nighttime nitrate radical in Hefei, China, *J. Environ. Sci.-China*, 20, 45–49, 2008.
- Lu, R. and Turco, R. P.: Air Pollutant Transport in a Coastal Environment.2. 3-Dimensional Simulations over Los-Angeles Basin, *Atmos. Environ.*, 29, 1499–1518, 1995.
- Lu, R. and Turco, R. P.: Ozone distributions over the Los Angeles basin: Three-dimensional simulations with the SMOG model, *Atmos. Environ.*, 30, 4155–4176, 1996.
- Lu, R., Turco, R. P., Stolzenbach, K., Friedlander, S. K., Xiong, C., Schiff, K., Tiefenthaler, L., and Wang, G. Y.: Dry deposition of airborne trace metals on the Los Angeles Basin and adjacent coastal waters, *J. Geophys. Res.-Atmos.*, 108, 4074, doi:10.1029/2001JD001446, 2003.
- Marchand, M., Bekki, S., Hauchecorne, A., and Bertaux, J. L.: Validation of the self-consistency of GOMOS NO₃, NO₂ and O₃ data using chemical data assimilation, *Geophys. Res. Lett.*, 31, L10107, doi:10.1029/2004GL019631, 2004.
- Matsumoto, J., Imagawa, K., Imai, H., Kosugi, N., Ideguchi, M., Kato, S., and Kajii, Y.: Nocturnal sink of NO_x via NO₃ and N₂O₅ in the outflow from a source area in Japan, *Atmos. Environ.*, 40, 6294–6302, 2006.
- Mihelcic, D., Klemp, D., Musgen, P., Patz, H. W., and Volzthomas, A.: Simultaneous Measurements of Peroxy and Nitrate Radicals at Schauinsland, *J. Atmos. Chem.*, 16, 313–335, 1993.
- Nakayama, T., Ide, T., Taketani, F., Kawai, M., Takahashi, K., and Matsumi, Y.: Nighttime measurements of ambient N₂O₅, NO₂, NO and O₃ in a sub-urban area, Toyokawa, Japan, *Atmos. Environ.*, 42, 1995–2006, 2008.
- Noxon, J. F., Norton, R. B., and Henderson, W. R.: Observation of atmospheric NO₃, *Geophys. Res. Lett.*, 5, 675–678, 1978.
- Noxon, J. F., Norton, R. B., and Henderson, W. R.: Comment on the problem of nighttime stratospheric NO₃ by Herman, J. R., *J. Geophys. Res.-Ocean. Atmos.*, 85, 4556–4557, 1980.
- Osterman, G. B., Salawitch, R. J., Sen, B., Toon, G. C., Stachnik, R. A., Pickett, H. M., Margitan, J. J., Blavier, J. F., and Peterson, D. B.: Balloon-borne measurements of stratospheric radicals and their precursors: Implications for the production and Loss of ozone, *Geophys. Res. Lett.*, 24, 1107–1110, 1997.
- Park, R. J., Jacob, D. J., Field, B. D., Yantosca, R. M., and Chin, M.: Natural and transboundary pollution influences on sulfate-nitrate-ammonium aerosols in the United States: Implications for policy, *J. Geophys. Res.-Atmos.*, 109, D15204, doi:10.1029/2003JD004473, 2004.
- Penkett, S. A., Burgess, R. A., Coe, H., Coll, I., Hov, ., Lindskog, A., Schmidbauer, N., Solberg, S., Roemer, M., Thijsse, T., Beck, J., and Reeves, C. E.: Evidence for large average concentrations of the nitrate radical (NO₃) in Western Europe from the HANSA hydrocarbon database, *Atmos. Environ.* 41, 3465–3478, 2007.
- Platt, U. and Stutz, J.: *Differential Optical Absorption Spectroscopy: Principles and Applications*, Springer, Berlin, Heidelberg, 2008.
- Platt, U., Perner, D., Winer, A. M., Harris, G. W., and Pitts, J. N.: Detection of NO₃ in the Polluted Troposphere by Differential Optical-Absorption, *Geophys. Res. Lett.*, 7, 89–92, 1980.
- Platt, U., Perner, D., Schröder, J., Kessler, C., and Toennissen, A.: The Diurnal Variation of NO₃, *J. Geophys. Res.*, 86, 11965–11970, 1981.
- Popp, P. J., Northway, M. J., Holecek, J. C., Gao, R. S., Fahey, D. W., Elkins, J. W., Hurst, D. F., Romashkin, P. A., Toon, G. C., Sen, B., Schauffler, S. M., Salawitch, R. J., Webster, C. R., Herman, R. L., Jost, H., Bui, T. P., Newman, P. A., and Lait, L. R.: Severe and extensive denitrification in the 1999–2000 Arctic winter stratosphere, *Geophys. Res. Lett.*, 28, 2875–2878, 2001.
- Ramsay, D. A.: Optical spectra of gaseous free radicals, in: *Xth Colloquium Spectroscopium Internationale, Proceedings*, Lippincott E. R. and Margoshes M., Spartan Books, Washington, D.C., 1963.
- Randel, W. J., Wu, F., Russell, J. M., and Waters, J.: Space-time patterns of trends in stratospheric constituents derived from UARS measurements, *J. Geophys. Res.-Atmos.*, 104, 3711–3727, 1999.
- Ravishankara, A. R. and Mauldin, R. L.: Temperature-Dependence of the NO₃ Cross-Section in the 662-nm Region, *J. Geophys. Res.-Atmos.*, 91, 8709–8712, 1986.
- Ravishankara, A. R. and Wine, P. H.: Absorption Cross-Sections for NO₃ between 565 and 673 nm, *Chem. Phys. Lett.*, 101, 73–78, 1983.
- Remedios, J. J., Leigh, R. J., Waterfall, A. M., Moore, D. P., Sembhi, H., Parkes, I., Greenhough, J., Chipperfield, M.P., and Hauglustaine, D.: MIPAS reference atmospheres and comparisons to V4.61/V4.62 MIPAS level 2 geophysical data sets, *Atmos. Chem. Phys. Discuss.*, 7, 9973–10017, doi:10.5194/acpd-7-9973-2007, 2007.
- Renard, J. B., Taupin, F. G., Riviere, E. D., Pirre, M., Huret, N., Berthet, G., Robert, C., Chartier, M., Pepe, F., and George, M.: Measurements and simulation of stratospheric NO₃ at mid and high latitudes in the Northern Hemisphere, *J. Geophys. Res.-Atmos.*, 106, 32387–32399, 2001.
- Rinsland, C. P., Salawitch, R. J., Gunson, M. R., Solomon, S., Zander, R., Mahieu, E., Goldman, A., Newchurch, M. J., Irion, F. W., and Chang, A. Y.: Polar stratospheric descent of NO_y and CO and Arctic denitrification during winter 1992–1993, *J. Geophys. Res.-Atmos.*, 104, 1847–1861, 1999.
- Röckmann, T., Rhee, T. S., and Engel, A.: Heavy hydrogen in the stratosphere, *Atmos. Chem. Phys.*, 3, 2015–2023, doi:10.5194/acp-3-2015-2003, 2003.
- SAGE III Algorithm Theoretical Basis Document: Transmission Level 1B Products, LaRC 475-00-108 v2.1, 26 March 2002.
- Salby, M. L.: Survey of Planetary-Scale Traveling Waves—the State of Theory and Observations, *Rev. Geophys.*, 22, 209–236, 1984.
- Sander, S. P.: Temperature-dependence of the NO₃ absorption-spectrum, *J. Phys. Chem.*, 90, 4135–4142, 1986.
- Sander, S. P., Friedl, R. R., Golden, D. M., Kurylo, M. J., Huie, R. E., Orkin, V. L., Moortgat, G. K., Ravishankara, A. R., Kolb, C. E., Molina, M. J., and Finlayson-Pitts, B. J.: Chemical Ki-

- netics and Photochemical Data for Use in Atmospheric Studies, Evaluation Number 14, JPL Publication 02-25, Jet Propulsion Laboratory, Pasadena, 2003.
- Sander, S. P., Finlayson-Pitts, B. J., Friedl, R. R., Golden, D. M., Huie, R. E., Keller-Rudek, H., Kolb, C. E., Kurylo, M. J., Molina, M. J., Moortgat, G. K., Orkin, V. L., Ravishankara, A. R., and Wine, P. H.: Chemical Kinetics and Photochemical Data for Use in Atmospheric Studies, Evaluation Number 15, JPL Publication 06-2, Jet Propulsion Laboratory, Pasadena, 2006.
- Sen, B., Toon, G. C., Osterman, G. B., Blavier, J. F., Margitan, J. J., Salawitch, R. J., and Yue, G. K.: Measurements of reactive nitrogen in the stratosphere, *J. Geophys. Res.-Atmos.*, 103, 3571–3585, 1998.
- Smith, J. P. and Solomon, S.: Atmospheric NO₃ 3. Sunrise disappearance and the stratospheric profile, *J. Geophys. Res.-Atmos.*, 95, 13819–13827, 1990.
- Smith, J. P., Solomon, S., Sanders, R. W., Miller, H. L., Perliski, L. M., Keys, J. G., and Schmeltekopf, A. L.: Atmospheric NO₃ 4. Vertical profiles at middle and polar latitudes at sunrise, *J. Geophys. Res.-Atmos.*, 98, 8983–8989, 1993.
- Smith, N., Plane, J. M. C., Nien, C. F., and Solomon, P. A.: Night-time Radical Chemistry in the San-Joaquin Valley, *Atmos. Environ.*, 29, 2887–2897, 1995.
- Solomon, S., Miller, H. L., Smith, J. P., Sanders, R. W., Mount, G. H., Schmeltekopf, A. L., and Noxon, J. F.: Atmospheric NO₃ 1. Measurement technique and the annual cycle at 40-degrees-N, *J. Geophys. Res.-Atmos.*, 94, 11041–11048, 1989.
- Stutz, J. and Platt, U.: Numerical analysis and estimation of the statistical error of differential optical absorption spectroscopy measurements with least-squares methods, *Appl. Optics*, 35, 6041–6053, 1996.
- Stutz, J., Alicke, B., Ackermann, R., Geyer, A., White, A., and Williams, E.: Vertical profiles of NO₃, N₂O₅, O₃, and NO_x in the nocturnal boundary layer: 1. Observations during the Texas Air Quality Study 2000, *J. Geophys. Res.-Atmos.*, 109, D12306, doi:10.1029/2003JD004209, 2004.
- Toon, G. C.: The JPL MkIV Interferometer, *Optics Photonics News*, 2, 19–21, 1991.
- Thomason, L. W., Poole, L. R., and Deshler, T.: A global climatology of stratospheric aerosol surface area density deduced from stratospheric aerosol and gas experiment II measurements: 1984–1994, *J. Geophys. Res.-Atmos.*, 102, 8967–8976, 1997.
- von Friedeburg, C., Wagner, T., Geyer, A., Kaiser, N., Vogel, B., Vogel, H., and Platt, U.: Derivation of tropospheric NO₃ profiles using off-axis differential optical absorption spectroscopy measurements during sunrise and comparison with simulations, *J. Geophys. Res.-Atmos.*, 107, 4168, doi:10.1029/2001JD000481, 2002.
- Vrekoussis, M., Mihalopoulos, N., Gerasopoulos, E., Kanakidou, M., Crutzen, P. J., and Lelieveld, J.: Two-years of NO₃ radical observations in the boundary layer over the Eastern Mediterranean, *Atmos. Chem. Phys.*, 7, 315–327, doi:10.5194/acp-7-315-2007, 2007.
- Wamsley, P. R., Elkins, J. W., Fahey, D. W., Dutton, G. S., Volk, C. M., Myers, R. C., Montzka, S. A., Butler, J. H., Clarke, A. D., Fraser, P. J., Steele, L. P., Lucarelli, M. P., Atlas, E. L., Schauffler, S. M., Blake, D. R., Rowland, F. S., Sturges, W. T., Lee, J. M., Penkett, S. A., Engel, A., Stimpfle, R. M., Chan, K. R., Weisenstein, D. K., Ko, M. K. W., and Salawitch, R. J.: Distribution of halon-1211 in the upper troposphere and lower stratosphere and the 1994 total bromine budget, *J. Geophys. Res.-Atmos.*, 103, 1513–1526, 1998.
- Wang, H. J., Cunnold, D. M., Froidevaux, L. and Russell, J. M.: A reference model for middle atmosphere ozone in 1992–1993, *J. Geophys. Res.-Atmos.*, 104, 21629–21643, 1999.
- Wang, S., Ackermann, R., and Stutz, J.: Vertical profiles of O₃ and NO_x chemistry in the polluted nocturnal boundary layer in Phoenix, AZ: I. Field observations by long-path DOAS, *Atmos. Chem. Phys.*, 6, 2671–2693, doi:10.5194/acp-6-2671-2006, 2006.
- Wang, S. H., Pickett, H. M., Pongetti, T. J., Cheung, R., Yung, Y. L., Shim, C., Li, Q. B., Canty, T., Salawitch, R. J., Jucks, K. W., Drouin, B., and Sander, S. P.: Validation of Aura Microwave Limb Sounder OH measurements with Fourier Transform Ultraviolet Spectrometer total OH column measurements at Table Mountain, California, *J. Geophys. Res.-Atmos.*, 113, D22301, doi:10.1029/2008JD009883, 2008.
- Wayne, R. P., Barnes, I., Biggs, P., Burrows, J. P., Canosamas, C. E., Hjorth, J., Lebras, G., Moortgat, G. K., Perner, D., Poulet, G., Restelli, G., and Sidebottom, H.: The Nitrate Radical—Physics, Chemistry, and the Atmosphere, *Atmos. Environ. A-Gen.*, 25, 1–203, 1991.
- Weaver, A., Solomon, S., Sanders, R. W., Arpag, K. and Miller, H. L.: Atmospheric NO₃ 5. Off-axis measurements at sunrise: Estimates of tropospheric NO₃ at 40° N, *J. Geophys. Res.-Atmos.*, 101, 18605–18612, 1996.
- Wu, D. L. and Waters, J. W.: Satellite observations of atmospheric variances: A possible indication of gravity waves, *Geophys. Res. Lett.*, 23, 3631–3634, 1996.
- Wu, S. L., Mickley, L. J., Jacob, D. J., Logan, J. A., Yantosca, R. M., and Rind, D.: Why are there large differences between models in global budgets of tropospheric ozone?, *J. Geophys. Res.-Atmos.*, 112, D05302, doi:10.1029/2006JD007801, 2007.
- Yang, E.-S., Cunnold, D. M., Salawitch, R. J., McCormick, M. P., Russell III, J., Zawodny, J. M., Oltmans, S., and Newchurch, M. J.: Attribution of recovery in lower-stratospheric ozone, *J. Geophys. Res.*, 111, D17309, doi:10.1029/2005JD006371, 2006.
- Yokelson, R. J., Burkholder, J. B., Fox, R. W., Talukdar, R. K., and Ravishankara, A. R.: Temperature-dependence of the NO₃ absorption-spectrum, *J. Phys. Chem.*, 98, 13144–13150, 1994.